IUTAM Symposium on *Critical flow dynamics involving moving/deformable structures with design applications*, June 18-22, 2018, Santorini, Greece

Smart Morphing and Sensing for the Wings of the Future

A. MAROUF[1,2], N. SIMIRIOTIS[2], J.B. TÔ[2], M. CARVALHO, Y. BMEGAPTCHE[2], A. KITOUNI[4] Y. HOARAU[1], J.F. ROUCHON[3], M. BRAZA[2]
[1]ICUBE – Strasbourg-France
[2]IMFT-Toulouse-France
[3]LAPLACE-Toulouse-France
[4]CEMENTYS-France

Abstract. This article presents a synthesis of main results from the H2020 European Research project N° 723402 "Smart Morphing and Sensing for Aeronautical Configurations", www.smartwing.org/SMS/EU concerning the design of disruptive wing configurations able to considerably increase the aerodynamic performances comparing conventional designs. This is achieved thanks to novel smart actuators electrically actuated and embedded under the "skin" of the lifting structure and new generation of sensors based on Bragg grating. Therefore, optimal deformations and vibrations are produced in multiple time and length scales, able to manipulate the surrounding turbulence structure in order to increase lift and simultaneously decrease drag and aerodynamic noise in all flight phases, take-off, landing and cruise.
Results from High-Fidelity numerical simulations accompanied by experiments with the morphing wing configurations of A3xx type are discussed regarding the increase of the aerodynamic performances.

Key words: electroactive morphing, vibration, trailing-edge, simulation, wings, aerodynamic.

1. Introduction

Trailing-edge high-lift devices have been widely used on many kinds of aircraft previously. The structure-deformation technology has also been regarded as promising in the field of aircraft design. Traditional high-lift devices have a precedent of using the concept of deformation, which is mainly applied to the rear of wing, in order to improve the performance of take-off and landing and this concept enables the manipulation of the near-region turbulence enhancing specific beneficial structures in the wake. In this way and thanks to the introduction of smaller-scale chaotic turbulent vortices, breaking down or suppression of pre-existing predominant instability modes can be achieved. This study is a part of electroactive morphing activities in the context of the SMS (Smart Morphing and Sensing) European project (www.smartwing.org/SMS/EU). It includes numerical simulations and physical analysis issued from the hybrid morphing, operating different time scales and associating different smart actuation approaches. This article focuses on a morphing A320 wing in clean configuration as well as on the high-lift wing-morphing flap in take-off of an Airbus A320 type configuration at high Reynolds number, using adopted turbulence modelling. This design using smart material properties in interaction with fluid flow aims at simultaneously increasing the lift, reducing the drag and the aerodynamic noise of the aircraft wings of the future. The morphing applied is partly bio-inspired. Optimal vibration and slight deformation of the trailing edge region by using smart piezo-actuators have been studied. The camber control is achieved by Shape memory Alloys (SMA) operating at low frequencies (order of 1 Hz), whereas the trailing-edge vibration are of higher order (100-500 Hz). The association of both actuations yielded to the *hybrid electroactive morphing*, term derived from the activities of the

multidisciplinary research group, (G. Jodin et al 2017), Scheller 2015) of the two French laboratories IMFT and LAPLACE running the morphing platform www.smartwing.org. The actuation of MFC (Micro-Fiber Composite) piezo-patches in the trailing edge region is simulated by using an amplitude of the vibration at 0.35 mm and a frequency range of [20-500 Hz]. The numerical studies have been accomplished in strong synergy with the experimental studies of the SMS project and contributed to the understanding of the physics and the performance of morphing. The present study uses advanced numerical simulation approaches implemented in our research team and used elsewhere in the European research institutes and aeronautical industry. A first part of the study concerns simulations and comparisons with the experiments around the "Reduced Scale (RS) prototype of the SMS project. The second part concerns the two-element A320 wing-flap "Large Scale" (LS) prototype of the SMS project in take-off configuration with cambered shapes and vibrating trailing edge through optimal actuations. A final synthesis of the aerodynamic performance increase is provided in the conclusions.

2. Flow configurations

The subsonic flow over the RS prototype has been investigated numerically and experimentally at Reynolds number of 1 Million and angle of incidence 10°. Fig. 1 shows this prototype with embedded SMAs and near- trailing edge piezoactuators. The wing was mounted wall-to-wall in the wind tunnel S4 of IMFT.

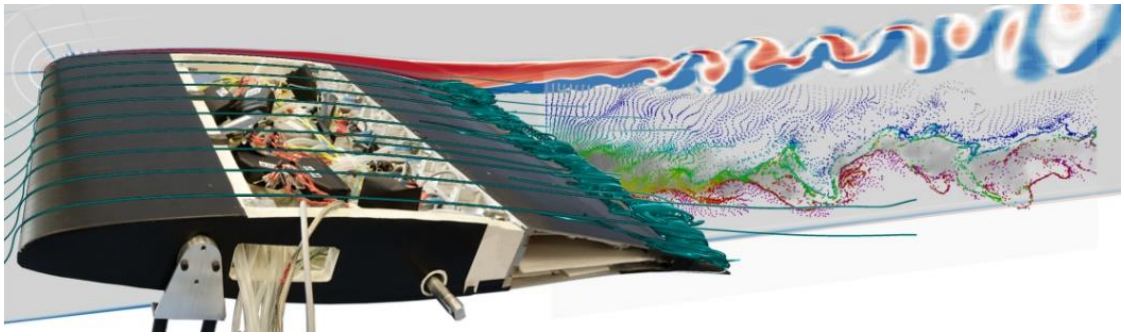

Figure 1: The RS (Reduced Scale) morphing A320 prototype

The LS prototype (wing/flap in take-off position) is shown in Figure 2, investigated numerically and experimentally in the S1 wind tunnel of IMFT for Reynolds numbers of 2.25 to 7 million. The total chord in take-off is 2.72m. An angle of attack $\alpha = 8.2°$ has been chosen corresponding to real high angles of take-off configurations.

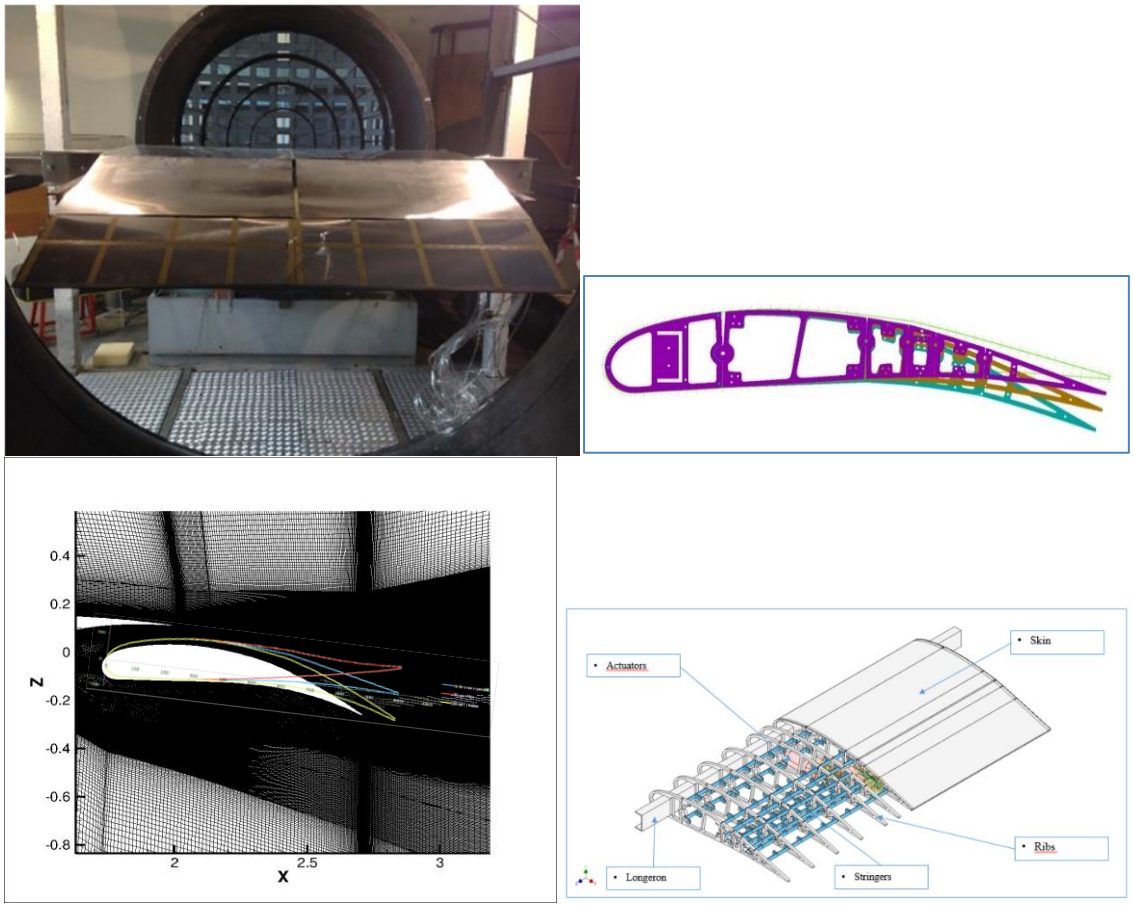

Figure 2: The LS wing/flap high lift prototype in the S1 wind tunnel of IMFT and of the morphing flap; cambering shapes investigated (left-bottom); view of the grid area in the gap region and around the high lift flap (right-top).

3. Numerical method and turbulence modelling

The simulations of the A320 in take-off position have been carried out with the Navier-Stokes Multi-Block (NSMB) solver (Hoarau et al, 2016).

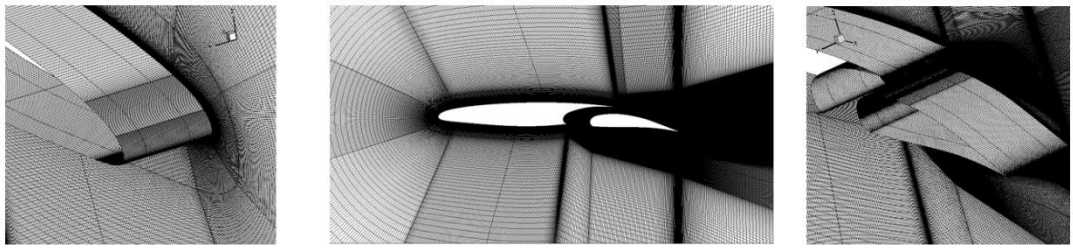

Figure 3: Grid details around the two-element configuration

Two multiblock grids of C-H topology in two dimensions and sizes of 0.5 M and 0.6 M cells have been examined. The results are very similar for the two grids. The finer grid has been used for the results of the study.
Furthermore, a Chimera grid has been used that contains two independent grids, the first being the fluid domain including the wing and the second one is around the flap (Fig.4) .

The Chimera grid is used for optiona configurations of Take-off and Landing where the flap changes its deflection angle from 10° to 40° degrees.

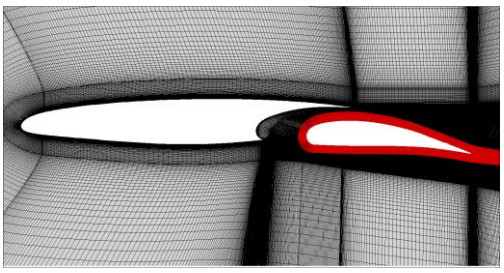

Figure 4: Presentation of Chimera grid.

The geometry's movement is taken into account through the ALE (Arbitrary Lagrangian Eulerian) formulation (Donea et al, 1982). The formulation adopted in the NSMB code adapts to discretized conservational equations using the finite volume method. The motion and slight deformation of the near-trailing edge region within a large vibraton frequency and amplitude ranges has been implemented in the same kind as in the experiments of the SMS project.

Concerning the turbulence modelling, The OES (Organised-Eddy Simulation) approach developed in our research group, (Braza *et al* 2006, Bourguet et al (2008), Szubert et al 2015, Simiriotis et al, 2019), able to sensitize the coherent structures development, has been employed. This modelling provides correct flow detachment including the separated shear layers and wake's vortex dynamics. In the present study this turbulence modelling approach has shown a clear appearance of the shear layer instability and of its the Kelvin-Helmholtz vortices formed in the upper and lower shear layers, leading to the von Kármán vortex shedding farther downstream. These aspects are crucial for the modification of these dynamics thanks to morphing and are well captured by the present approach. The refined mesh has around 250 cells within a distance of two chords downstream of the trailing edge, able to capture smaller scale eddies with a size around 1.5cm~2cm.

The y^+ length regarding the turbulence modelling near the wall is smaller than 0.5 in the whole domain.

4. Results

4.1 The RS prototype

The results around the RS prototype are shown in fig.5 by using a 60 Millon grid. Fgure 5 shows the 3D structure around the wing as well as the coherent and smaller scale vortices along the span. Vortex dislocations (Braza et al, 2001) are formedand interact with the streamwise vorticity.

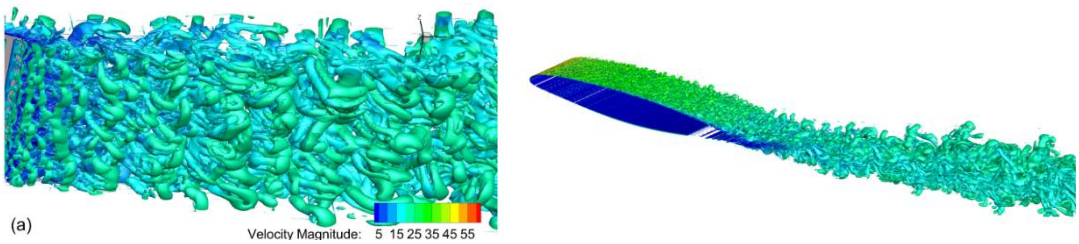

Figure 5: Velocity magnitude contours showing the spanwise secondary instability and the streamwise vortex pattern.

After a detailed parametric study in the range of 60 to 500 Hz vibrations through the piezoactuators, an optimal range of the actuation frequency around 300 Hz has been detected, leading to suppression of the three-dimensionality and of vortex dislocations, thus reducing the *rms* of the forces.

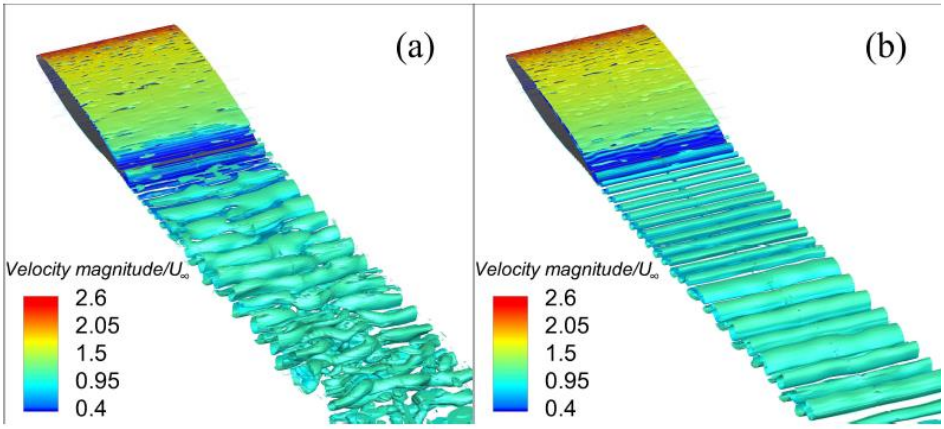

Figure 6: Velocity magnitude contours, RS A320 prototype, Re=1M, a=10°: left: static configuration (no morphing); right: morphing at optimal frequency of 300 Hz and slight deformation of the piezoactuators with an amplitude of 0.35mm

	CL	**CD**	**CL/CD**
Static	1.5646	0.0219	71.5
300 Hz	1.6147	0.0217	74.5 (4.2%)

Table 1: Lift and drag coefficients as well as L/D ratio compared to the static (non-morphing) case.

The increase of the aerodynamic performance is shown in Table 1. A 4.2% of increase has been obtained.

The *hybrid electroactive morphing* applying simultaneously cambering through SMA's and trailing edge vibrations has been studied experimentally and numerically.

Thanks to the cambering, manipulation of the shear - layer vortices *leads to refraining the augmentation of drag* that would occur because of the increase of the bluff-body's effect due to the cambering. Fig.7 shows through Tme-Resolved PIV (TRPV) the formation of the shear layer vortices downstream of the separation under dynamic cambering downwards, by means of SMA. It has been obtained that the trailing edge actuation adds a 2% more lift (Fg.8).

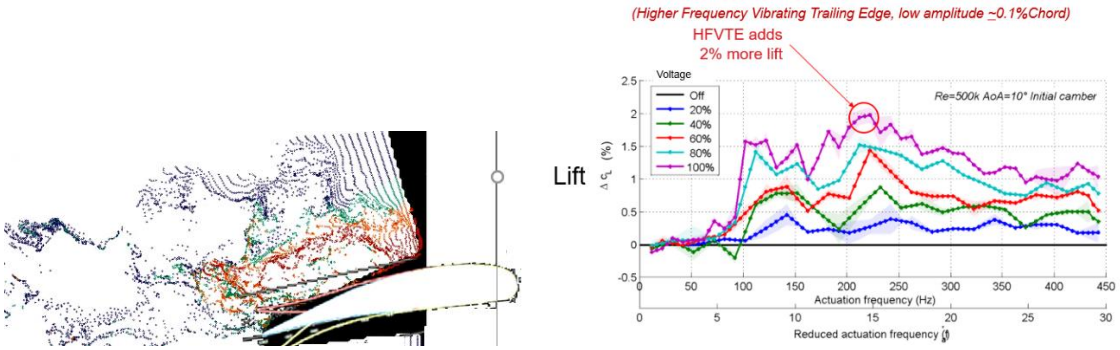

Figure 7: Left: TRPIV around the RS prototype in dynamic cambering through SMA actuators in the S4 wind tunnel of IMFT; right: Higher frequency vibrating trailing edge actuation.

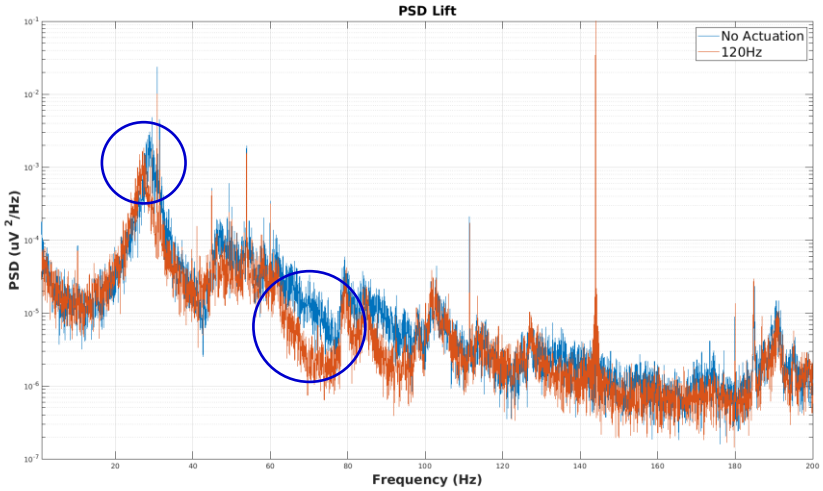

Figure 8: PSD (Power Spectral Density) of the lift coefficient measured by aerodynamic balance: effect of morphing through trailing edge vibration (red), comparing to the static case (blue).

Simultaneously with the aerodynamic performance increase, the present morphing through selected vibrations leads to reduction of the predominant frequency modes and of the turbulence energy, producing trailing edge noise, by an order of 20 dB.

The transonic tRS prototype

This prototype of the SMS project has been designed to respect the dimensions of 0.15 m chord and span regarding the wind tunnel of IMP-PAN (Gdansk, Poland) partner of the SMS project. The simulations respected these dimensions. The inlet Mach number is 0.78 and the incidence of 1°.8 respecting the operation conditions in cruise.
The simulations show through streaklines (fig.) the importance of the feedback effects from the flow unsteadiness downstream of the shock-boundary layer interaction, (SBLI) that affects even the areas upstream of the SBLI, where the flow reversal produces a slight thickening of the boundary layer and creates the secondary oblique weak shock wave upstream of the main SBLI.

A large parametric study of the vibrations and amplitudes near the trailing edge has been accomplished and determined optimal ranges in the interval of 300 - 350 Hz. Indeed, this actuation is able to manipulate adequately the near-wake unsteadiness and to suppress the coherent structures, leading to a drag reduction of order 9% and a L/D increase of order 6%.

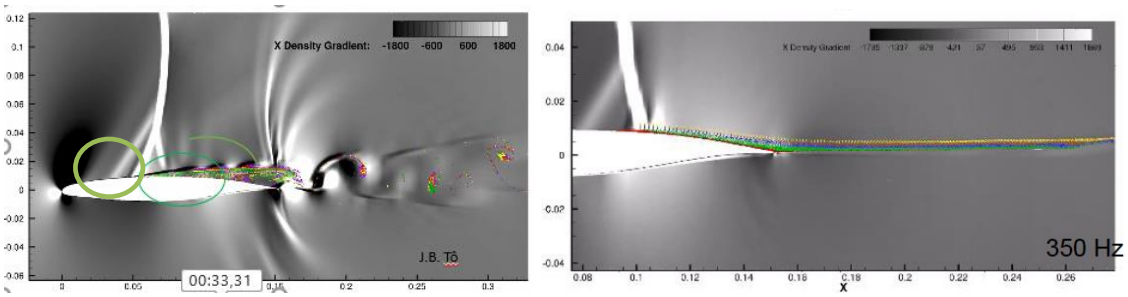

Figure 9: Static trS prototype ; left: streaklines showing the shear layer and near wake unsteadiness in interaction with the SBLI and the feedback effect; right: Suppression of the coherent eddies and thinning of the wake's width through optimal actuation.

Frequency (Hz)	100	150	200	250	300	350	400	450
$(\langle C_d\rangle - \langle C_d\rangle_{static}) \times 100/\langle C_d\rangle_{static}$	-0.21%	-0.84%	4.71%	-2.07%	-3.47%	-8.87%	6.11%	12.33%
$(\langle C_l\rangle - \langle C_l\rangle_{static}) \times 100/\langle C_l\rangle_{static}$	-0.83%	-0.63%	2.73%	-0.74%	-1.10%	-3.84%	3.45%	6.12%
$(\langle C_l/C_d\rangle - \langle C_l/C_d\rangle_{static}) \times 100/\langle C_l/C_d\rangle_{static}$	-0.62%	0.20%	-1.89%	1.33%	2.46%	5.51%	-2.52%	-5.50%

Table 2: Aerodynamic performance in cruise

The LS prototype

The results around the LS prototype are discussed in the following.
Figure 2 shows the prototype mounted in the S1 wind tunnel of IMFT, having a 2.50 m test section. The LS prototype's cambering is realised experimentally by SMAs and Electromechanical actuators. Optimal cambering forms studied in the SMS project (fig.2) have been examined numerically.

Pressure measurements have been carried out in the S1 wind tunnel according a novel method based on Bragg grating (Othonos 1997), realised by CEMENTYS partner of the SMS project. This allows simultaneous fluctuating pressure measurements at different positions, as shown in fig. 10. Moreover, the advantage of this method is its non-intrusive character thanks to the transducers ability to be embedded on the surface, without needing cavities. The PSD of fig. 10 shows capturing of the predominant frequency modes by this method in good agreement with the simulatons and pressure measurements by a Megitt pressure transducer (Figure 11).A good agreement with the numerical simulations is obtained. The pressures sensing has been used in the SMS project to create feedback control of the actuation system, mentioned in the final report of the project.

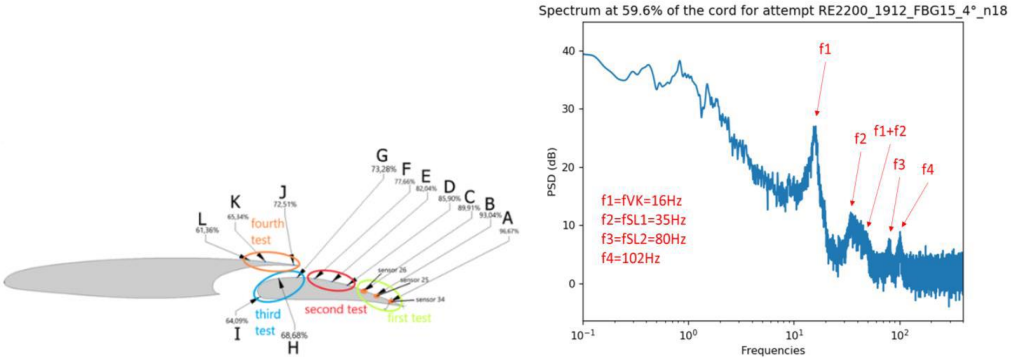

Figure 11: Location of simultaneous fluctuating pressure measurements in three groups (left); PSD of the Bragg grating transducers (right).

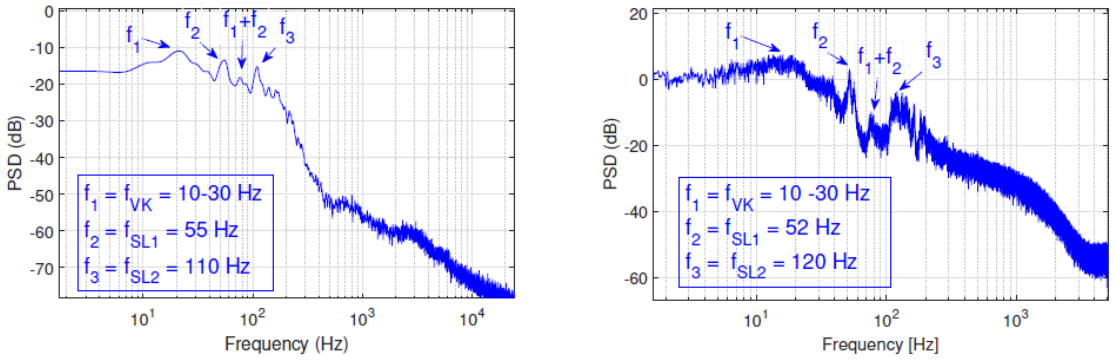

Figure 12: Comparison of the experimental spectra (left, Megitt pressure transducer) with the simulations (right).

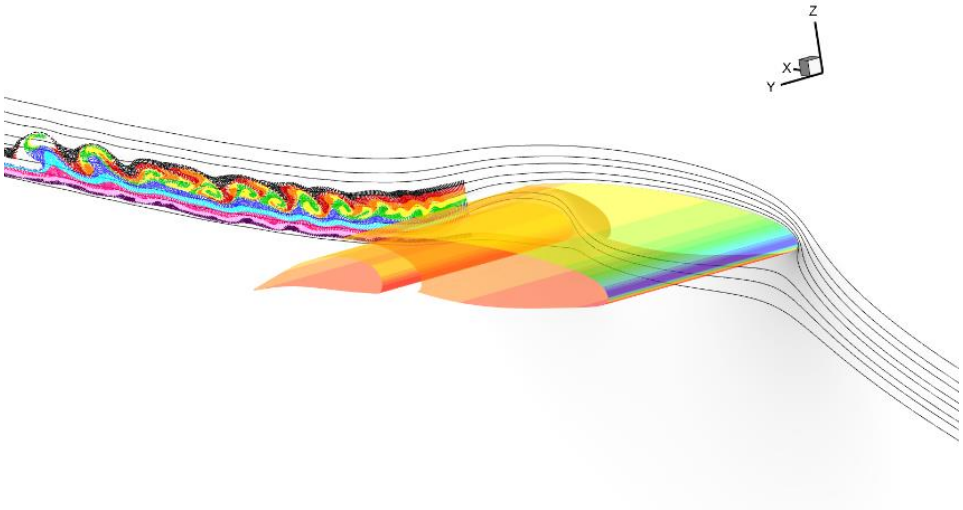

Figure 13: Streaklines and pressure on the surface of the A320 wing.

Figure 13 shows the streaklines and iso-pressure contours around the LS prototype, where the TNT (Turbulent-Non Turbulent) and TT (Turbulent-Turbulent) interfaces delimiting

the shear layer sand their interaction are shown, as well as the formation of Kelvin-Helmholtz vortices, providing farther downstream the von Kármán shedding.

Trailing-edge vibration and slight deformation effects

The electroactive morphing through mini-piezo-actuators disposed along the span near the trailing edge region creates vibrations and slight deformations (order of cm) with frequencies in the range of 30-500 Hz. It is shown in the present study that this kind of vibration has a has prominent effect on the development of the coherent vortex structures in the wake, on the wake's width and by feedback effect, on the aerodynamic forces, as shown in the following. The optimal results have been analysed concerning the higher-order range of the vibration frequency.

3.1 Wake instabilities

To a better understanding of the flow around the two wing-flap elements at the take-off position, we distinguish 3 elementary attached flow regions due to the presence of two objects in the flow (wing and flap), a separating area is noticed due to the presence of the gape Figure6. The presence of two different natural frequencies in the wake, a higher frequency of 80 ~ 90 Hz which corresponds to the Kelvin-Helmholtz vortices created near the flap and a lower frequency which is the half of the first 30Hz that correspond to the von Kármán instability, Figure7. Drawing the streaklines Figure4 it is clearly seen that this frequency corresponds to Kelvin Helmholtz instability.

The morphing manipulates the coherent vortex structures and produces vortex breakdown attenuating harmful ones, associated to drag and noise and enhance the coherent structures that are beneficial for the lift. These actions are achieved through the trailing edge vibration that produces smaller-scale vortices that trigger eddy-blocking effects (Szubert et al 2015) that constrict the shear layers and reduce the wake's width. The wake's instabilities and corresponding vortex structures are compared in the static and morphing cases. It has been found that vibration in low frequencies near the natural frequencies provide a slight modification of the flow. Actuation at higher frequencies near 300 Hz has shown ability of attenuation of the shear layer instability and of the corresponding coherent structures, Figure6.

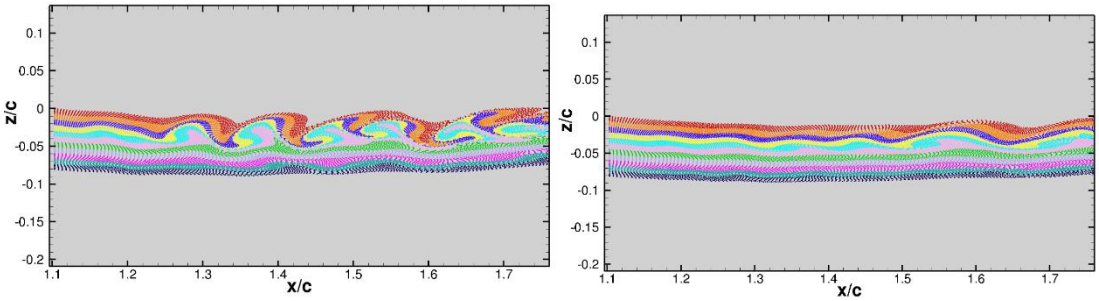

(a) (b)

Figure 14: Streaklines in the wake region, (a) : Static case. (b) : morphing case 300Hz.

The signal of the crossflow velocity component is extracted for 5 points from the static and morphing cases. The Figure7 shows the wake crossflow velocity field, that exhibit

the vortical structures. The monitor points are located in the wake close and far from the flap trailing edge.

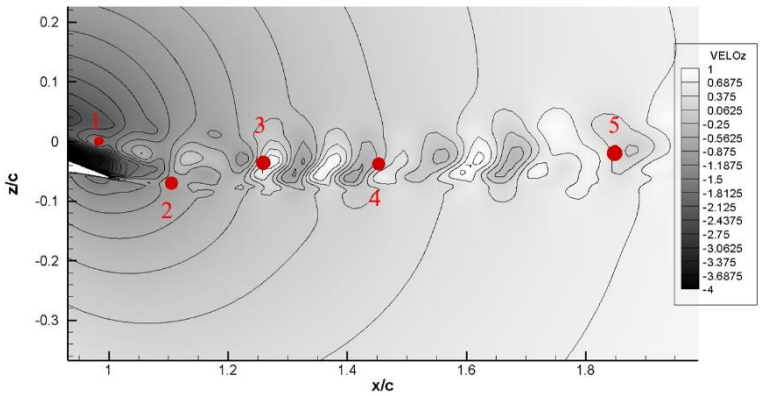

Figure 15: vertical velocity component iso-contours and monitor points for the spectral analysis

The PSDs are computed using the Welch's weighted overlapped segment averaging estimator (Welch, 1967 [7]), using Hamming windows with 50% overlap and zero padding. To show the Kelvin Helmholtz instability in the spectrum three points *3 (x/c=1.26), 4 (x/c=1.45)* and *5 (x/c=1.85)* have been selected to capture the predominant natural frequency in the wake, the frequency of the Kelvin Helmholtz is of the order of f_{SL} *= 30Hz.* Figure8 compares the PSD for the static and the actuating f_{act} =300Hz for the crossflow velocity one can see that the turbulent energy is reduced with increasing actuation frequency of actuation. This leads to a reduction of the size of the vortices Figure6. The shear layer mode, f_{SL} and also higher order frequencies are attenuated in the morphing case. In order to take a closer at the actuation effects on the flow the next section will decompose the flow in proper orthogonal modes to identify for each actuation frequency the most energetic structures.

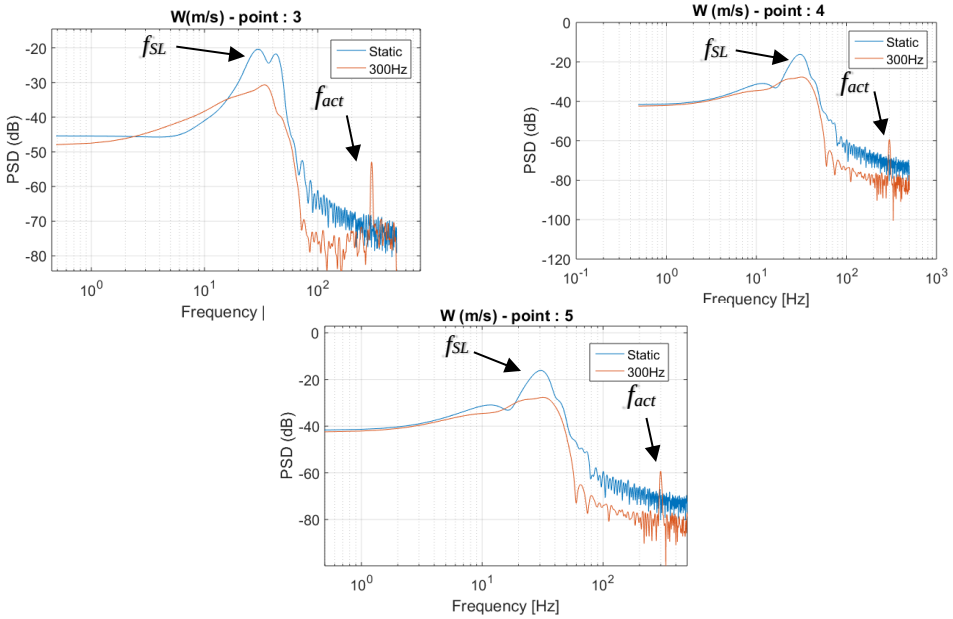

Figure 16: PSD of the crossflow velocity in the wake. The bump indicated by the first arrow corresponds to the wake instability modes.

4.2. Modal analysis

The Proper Orthogonal Decomposition (Karhunen & Loweve modes, Berkooz et al [8]) is applied to study the modification through the morphing occurred on the most energetic modes. The flow solution is decomposed into spatial ϕ_i modes and α_i temporal coefficients sorted by their relative energy in the flow.

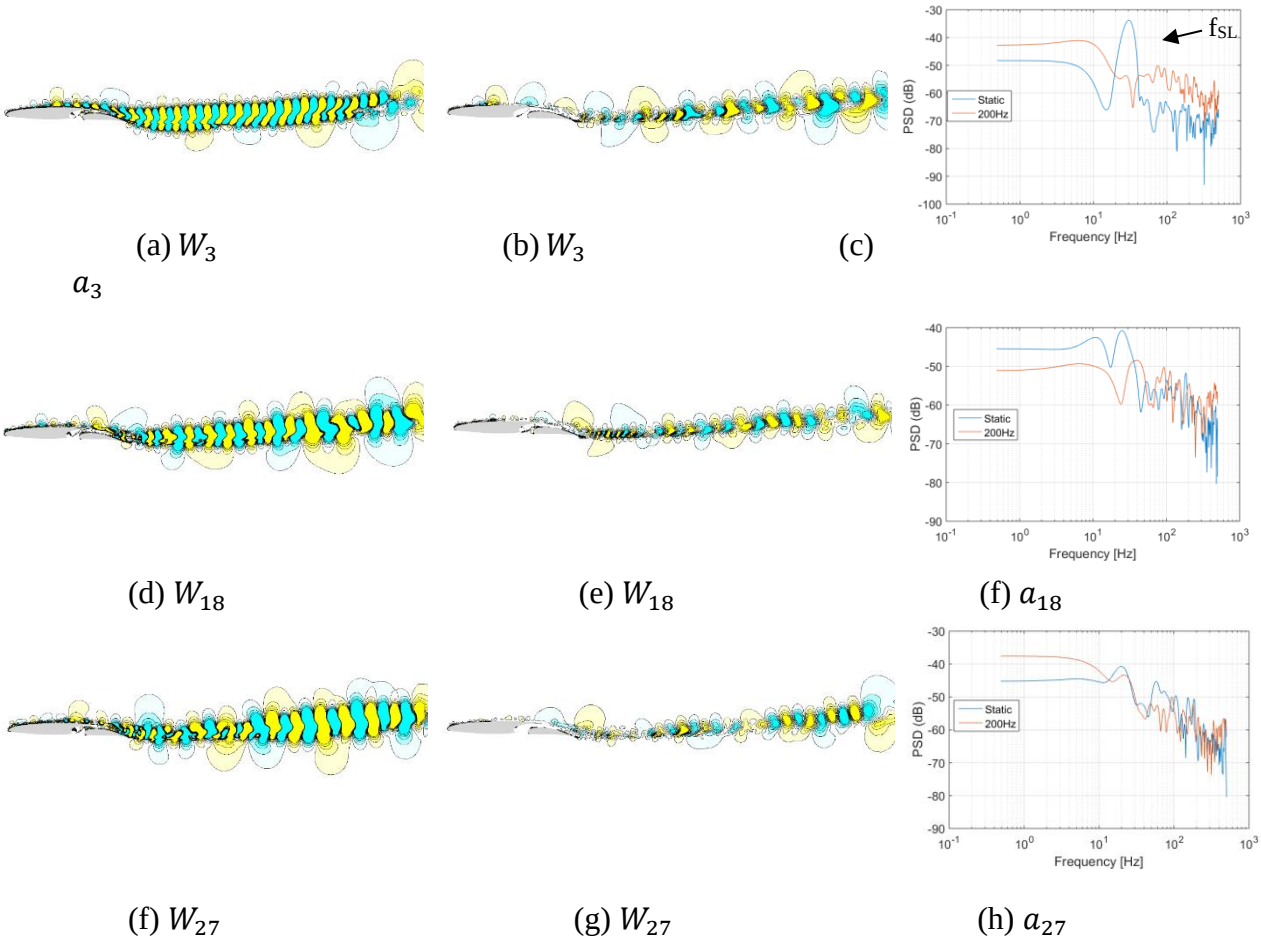

(a) W_3 (b) W_3 (c) a_3

(d) W_{18} (e) W_{18} (f) a_{18}

(f) W_{27} (g) W_{27} (h) a_{27}

Figure 17 : Spatial modes (*W*i)and PSD of the temporal coefficients computed for the crossflow velocity : static case (a), (d) and (f) and morphing case (b), (e) and (g) at 200Hz.

The time step of the sampling is $10^{-3}s$ which is less than inverse of the highest natural frequency on the wake. A constant number of snapshots (300) were used to construct the POD correlation matrix.

The spatial modes (shown in Figure 9) for the static and morphing cases is significantly different. The energy of the coherent structures in the wake is decreased. The actuation

introduces additional modes which supersede the frequency of the shear layer. This effect was also shown by experimental results of our group, (Johannes et al [9]). Furthermore, the temporal coefficients (fig.9) and their PSD (see for example a_3) underline this behaviour.

4.3. Time averaged results

The profiles of the mean axial velocity are compared for two x/c positions, (Figure 10)

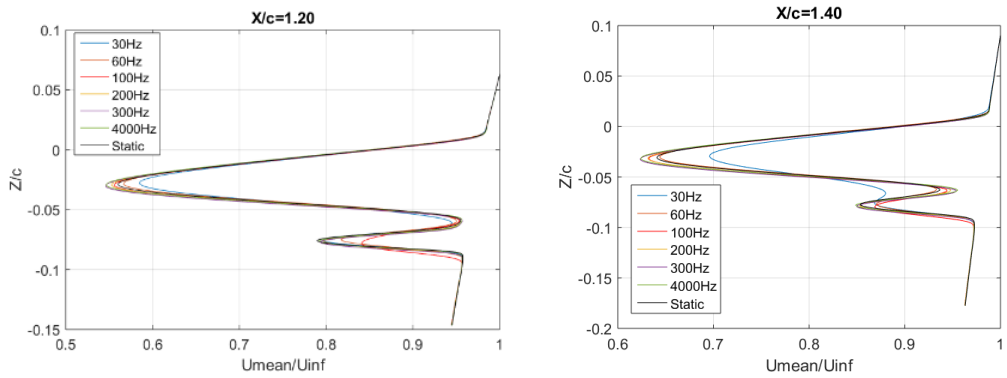

Figure 18: Time-averaged longitudinal velocity profiles along the wake for various actuating frequencies.

At the location *x/c=1.40*, the region of the gap is suppressed and a mixing between the two shear layers coming from the flap and the wing occurs. With an actuation frequency *100 Hz* the changes are important and the velocity deficit decreases ($U - U_{inf}$), thus reducing the skin friction gradient, $\tau = \mu\, \partial U/\partial y$.

	Position 1	Position 2	Position 3	Position 4
0°	**+ 13.76**	**+ 20.67**	**+ 22.67**	**+ 22.74**
2°	**+ 7.97**	**+ 10.35**	**+ 10.79**	**+ 10.41**
4°	**+ 3.26**	**+ 2.63**	**+1.21**	**+0.21**

Table 3: Numerical simulation of the aerodynamic performance (L/D) percentage modification for the cambered shapes, Re : 7M. $\frac{(CL/CD - CL_{ref}/CD_{ref})}{CL_{ref}/CD_{ref}}$ X 100

Table 3 shows the L/D aerodynamic performance by means of the cambered shapes shown in fig. xxx. Camber N°1 in 4° of incidence shows the best performance. IN Fig.

xxx this is compared to the reference take-off configuration (e.g) without morphing and higher angle of incidence), showing the benefits obtained through the morphing, that provides higher performance in lower angle of incidence.

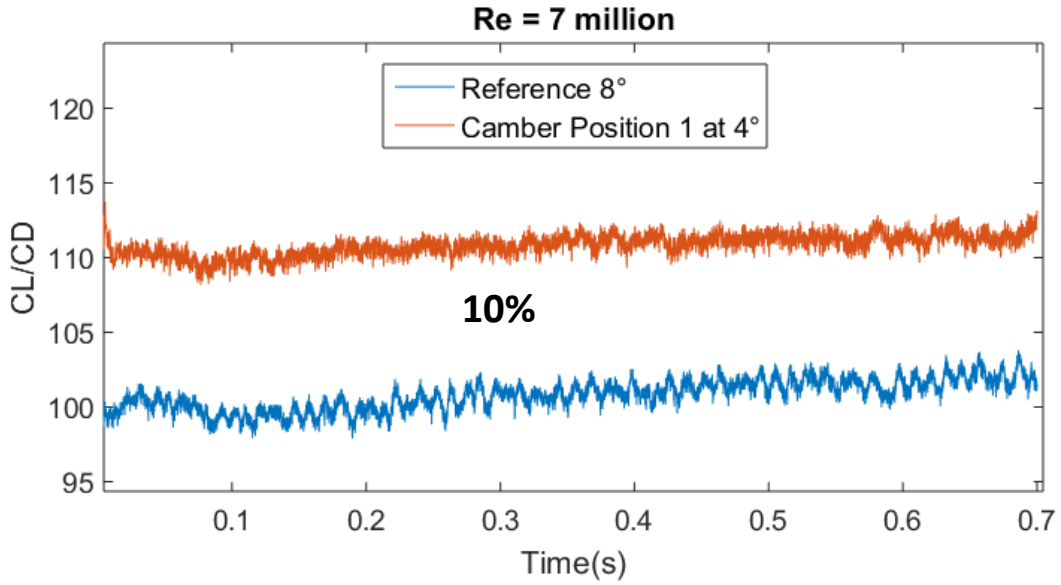

Figure 19: Aerodynamic performance thanks to morphing with camber position 1 at incidence of 4° comparing to the conventional (reference) design in take-off at 8°.

5. Conclusions

In this study the morphing effects through actuation operating at different time scales and vibration frequencies has been investigated. A significant aerodynamic performance increase has been obtained (order of 10%) by selected cambering shapes and optimal vibrations in low amplitudes in subsonic (take-off) and transonic (cruise) flight phases, where a drag reduction of order 9% has been provided.

Acknowledgements

This project has received funding from the European Union's H2020 program SMS, "Smart Morphing and Sensing for aeronautical configurations" under grant agreement No 723402. The computations have been carried out thanks to C.P.U. allocation of the French Supercomputing Centres CINES, CALMIP and TGCC as well as to the PRACE allocation No 2017174208 - project FWING.

References

1. Y. Hoarau, D. Pena, J. B. Vos, D. Charbonier, A. Gehri, M. Braza, T. Deloze, and E. Lau- rendeau. Recent Developments of the Navier Stokes Multi Block (NSMB) CFD solver. *In 54th AIAA Aerospace Sciences Meeting. American In- stitute of Aeronautics and Astronautics. DOI: 10.2514/6.2016-2056.*
2. J. Donea, S. Giuliani, and J. P. Halleux. An arbi-trary lagrangian-eulerian finite element method for transient dynamic fluid-structure interactions. *Computer Methods in Applied Mechanics and Engineer- ing, 33(1):689–723, September 1982*

3. R. Bourguet, M. Braza, G. Harran, and R. El Ak- oury. Anisotropic Organised Eddy Simulation for the prediction of non-equilibrium turbulent flows around bodies. *Journal of Fluids and Structures, 24(8):1240–1251, November 2008*
4. D. Szubert, F. Grossi, A. Jimenez Garcia, Y. Hoa- rau, J. C. R. Hunt, and M. Braza. Shock-vortex shear-layer interaction in the transonic flow around a supercritical airfoil at high Reynolds number in buffet conditions. *Journal of Fluids and Structures, 55:276–302, May 2015*
5. Welch, P.D., 1967. The use of fast Fourier transform for the estimation of power spectra: A method based on time averaging over short, modified periodograms. *IEEE Trans. Audio Electroacoust. 15 (2), 70–73.*
6. Berkooz, G., Holmes, P., Lumley, J.L., 1993. The proper orthogonal decomposition in the analysis of turbulent flows. *Annual Review of Fluid Mechanics25 (1), 539–575.*
7. J. Scheller, M. Chinaud, JF. Rouchon, E. Duhayon, S. Cazin, M. Marchal, M. Braza. Trailing-edge dynamics of a morphing NACA0012 aileron at high Reynolds number by high-speed PIV. *Journal of Fluids and Structures 55 (2015) 42–51.*
8. N. Simiriotis, G. Jodin, A. Marouf, P. Elyakime, Y. Hoarau, J.C. Hunt, J.F. Rouchon, M. Braza, "Morphing of a supercritical wing by means of trailing edge deformation and vibration at high Reynolds numbers: experimental and numerical investigation", J. Fluids & Structures, **91**, 2019. https://doi.org/10.1016/j.jfluidstructs.2019.06.016
9. A. Othonos, "Fiber Bragg gratings" ,Review of Scientific Instruments, 68, 4309-4341 (1997), DOI:http://dx.doi.org/10.1063/1.1148392